

Structural and electrical behavior of Ag nanolayer grown on graphene-doped ZrO₂ sheet

Hugo. P. A. Alves¹, Paulo. H. Chiberio², Marcio. A. Correa^{2,3}, Wilson. Acchar^{2,3}

¹*Department of Materials Science and Engineering, Federal University of Paraíba, 58051-900, João Pessoa, PB, Brazil*

²*Postgraduate Program in Materials Science and Engineering, Federal University of Rio Grande do Norte, 59078-970 Natal, RN, Brazil*

³*Department of Physics, Federal University of Rio Grande Do Norte, 59078-970, Natal, RN, Brazil*

Abstract

In this study, we report an experimental investigation of the structural, morphological, and electrical properties of the ZrO₂-Ag-Graphene sheet. In particular, we use the tape casting technique to produce the flexible ZrO₂ ceramic sheet and impregnation and magnetron sputtering techniques to incorporate graphene and silver. Structural and morphological analyses indicate the presence of graphene and silver in the ceramic matrix, confirming the methods efficiency. We noticed that with the deposition of graphene and silver on the ZrO₂ sheet, there is a decrease in electrical resistance. This fact is associated with the crystalline structure and morphology of graphene and silver, which makes sheets attractive in electrical applications. Thus, our results become fascinating for specific technological applications.

Keywords: ZrO₂-Ag-Graphene sheet; tape casting; impregnation; magnetron sputtering; electrical response.

INTRODUCTION

Zirconia-based electrical ceramic matrices have been the subject of recent research due to their diverse technological applications, such as optoelectronic devices [1], solid oxide fuel cells [2], capacitors [3], and cellular cells [4]. In this sense, the electrical properties of these materials have great potential in multifunctional technological applications [5–7].

To improve the electrical properties of ZrO₂ matrices, we highlight the deposition of carbon-based materials and the insertion of metallic materials, particularly silver (Ag). Ag is known for its excellent conductivity and low resistivity, making it an ideal candidate for electrode materials [8]. The growth of Ag nanolayers on graphene-doped ZrO₂ sheets not only leverages the inherent conductivity of Ag but also synergistically combines it with the improved conductivity and structural strength conferred by graphene [9, 10]. Incorporating Ag and graphene into ceramic matrices presents an opportunity to develop high-performance materials for various technological applications [11, 12]. For example, Ahmad et al. [13] observe that the optical properties of the ZnO ceramic matrix are affected by the incorporation of graphene and Ag, making them nanocomposites with potential for photocatalytic applications. In another study, Sadoun et al. [14] realize that doping graphene and Ag in the Al₂O₃ matrix modifies the mechanical properties, targeting structural applications.


In this sense, developing a flexible ceramic matrix for

the deposition of these materials allows the easy integration of the deposited components, enabling their broad functionalization [15, 16]. Tape casting [17], impregnation [18], and magnetron sputtering [19] techniques can produce these multilayers. The tape casting technique produces flexible ceramic sheets that can be shaped before sintering and allows multilayer structures [20, 21]. On the other hand, impregnation consists of the high adsorption capacity of the material deposited through the porosity, where deposition control can be controlled [22]. Now, the magnetron sputtering technique allows the growth of nanostructures in a single film or multilayer geometry, being grown on rigid, amorphous, or oriented substrates [23]. Few studies have been conducted regarding functionalizing the structural and electrical properties of nanostructures grown on ceramic sheet substrates decorated with carbon-based materials.

This study focuses on the structural and electrical behavior of a silver (Ag) nanolayer grown

on graphene-doped ZrO₂ sheets. By examining the interaction between the Ag nanolayer and the graphene-doped ZrO₂ substrate, we aim to elucidate how the inclusion of these nanostructures influences the electrical performance of the material. Specifically, microstructural characterization will be studied to understand the distribution and morphology of Ag particles on the composite surface. Therefore, this research aims to develop multifunctional materials with enhanced electrical properties, which can have wide applications in electronics, energy storage devices, and sensors. Understanding the interaction between the metallic nanolayers and the graphene-doped ZrO₂ substrate is essential to tailoring these composite materials for specific industrial applications, ensuring high performance and long-term stability.

*eng.hugoplinio@gmail.com

 <https://orcid.org/0000-0003-3408-943X>

EXPERIMENTAL PROCEDURE

As shown in Table 1, the preparation of the ceramic suspension occurred in two steps through the ball milling process, each lasting 24 h. Subsequently, the ceramic suspension was deposited on a polyethylene film using the TTC-1200 desktop tape casting machine (Tape Casting Warehouse, Inc.) at room temperature, with a 20.2 cm/min transport speed. The green sheet was dried in equipment at room temperature and in a controlled atmosphere for 24 h. The sheets were calcined (HT 17/04, Nabertherm, Lilienthal/Bremen, Germany) at 773 K under a heating rate of 0.5 K/min for 60 min to eliminate residual organic components and sintered at 1773 K with a heating rate of 5 K/min for 60 min.

The deposition of graphene (Sigma-Aldrich, with an average particle size of $\leq 2 \mu\text{m}$) on the ZrO_2 sheet was carried out using the impregnation technique. In this technique, graphene was dispersed in an isopropyl alcohol solution by ultrasound for 2 h to obtain a homogeneous mixture. Subsequently, the graphene solution was impregnated into the sheet and kept for 24 h at room temperature. On the other hand, silver (Ag) deposition occurred using the magnetron sputtering technique, where the sheet was placed on a glass substrate previously covered by a 2 nm Ta buffer with the following deposition parameters: base pressure of 8×10^{-8} Torr, Ar pressure during deposition of 2×10^{-3} Torr and DC of 25 mA.

Rheological characterization was measured using Haake Viscotester (Thermo Scientific, Thermo Fisher Scientific Inc.) with dual cone/plate geometry at room temperature. Thermogravimetric analysis (TGA) of the green leaf was performed (DTG-60, Shimadzu Corporation, Japan) with a temperature ranging from 298 K to 873 K, a heating rate of 3 K/min, and a flow rate of 50 mL/min. X-ray diffraction (XRD, MiniFlex II; Rigaku Corporation, Japan) was analyzed using Bragg-Brentano geometry ($\theta - 2\theta$) and $\text{Cu-K}\alpha$ radiation. The diffractograms were refined using the Rietveld method using MAUD software. Raman spectra were collected under ambient conditions on a WITec Access system using 633 nm (1.96 eV) as a pump laser. Scattered light was collected through a 50 \times objective using a 300 lines/mm grating in the backscatter configuration. Field emission scanning electron microscopy (FESEM) and energy dispersive spectrum (EDS) images were obtained using a Zeiss Auriga 40 microscope. Finally, the four-point probe method measured

electrical properties at room temperature using I-V curves (source measurement unit, model 238, Keithley).

RESULTS AND DISCUSSION

Fig. 1a shows the rheological analysis of the ceramic suspension used to prepare the sheet. We observed a decrease in viscosity with an increase in the shear rate, which is characteristic of the pseudoplastic behavior that prevents the settling of the particles and preserves a homogeneous distribution of the sheet components [24, 25]. Fig. 1b presents the thermal analysis of the flexible green sheet. We noticed a weight loss of 1.30 % between temperatures 385 K and 517 K and another of 16.39 % between temperatures 517 K and 650 K, which are related to the decomposition of organic constituents [26]. The third weight loss of 4.09 % between 650 K and 750 K temperatures is attributed to the decomposition of residual organic materials [27]. Therefore, the calcination temperature of 773 K becomes adequate.

In Fig. 1a, we observe a decrease in viscosity with increasing shear rate, characterizing a pseudoplastic behavior [24]. The thermal analysis of the green sheet, Fig. 1b, shows a weight loss of 1.30 % between the temperatures of 385 K and 517 K and another of 16.39 % between the temperatures of 517 K and 650 K, which are related to the composition of organic constituents [26]. A third weight loss of 4.09 % between 650 K and 750 K temperatures is attributed to the loss of residual organic materials [27].

The refined XRD patterns of the ZrO_2 -Ag-Graphene sheet, ZrO_2 sheet, and Ag powder are displayed in 1c. All diffraction peaks are associated with the phases: ZrO_2 with monoclinic symmetry (ICSD-60900 and space group P121/c1) [28], ZrO_2 with tetragonal symmetry (ICSD-68781 and space group P42/nmc) [29], and Ag with cubic symmetry (ICSD-64996 and space group Fm3m) [30]. The 2θ peaks of monoclinic ZrO_2 are at 28.19° and 31.41° , corresponding to the (11 $\bar{1}$) and (111) planes, with d-spacings of approximately 2.84 Å and 3.12 Å, respectively [31]. The planes corresponding to tetragonal ZrO_2 are (011), (110), (112), (013), (121), (022), (004), and (220), which are located at 2θ equal to 30.24° , 35.29° , 50.24° , 59.29° , 60.25° , 62.89° , 72.93° and 74.65° , with d-spacings of approximately 3.07 Å, 2.54 Å, 1.79 Å, 1.67 Å, 1.75 Å, 1.53 Å, 1.29 Å and 1.27 Å, respectively [32]. The existence of 2 θ peaks located at 38.25° , 44.12° , 64.27° and 77.52° , corresponding to the planes (111), (200), (220), and (311), indicates the formation of

Table 1 - Parameters used in the preparation of the ceramic suspension.

Step	Order	Material	Function	wt. %	Manufacturer
1	1	Distilled water	Solvent	22.0	-
	2	Darvan 821 A	Dispersant	1.0	Vanderbilt
	3	ZrO_2	Ceramic powder	55.0	Tosoh
2	1	Monowilith LDM – 6138	Binder	20.0	Clariant
	2	Antifoam A	Plasticizer	0.5	Sigma-Aldrich
	3	Coconut diethanolamine	Antiespumant	1.5	Stapan

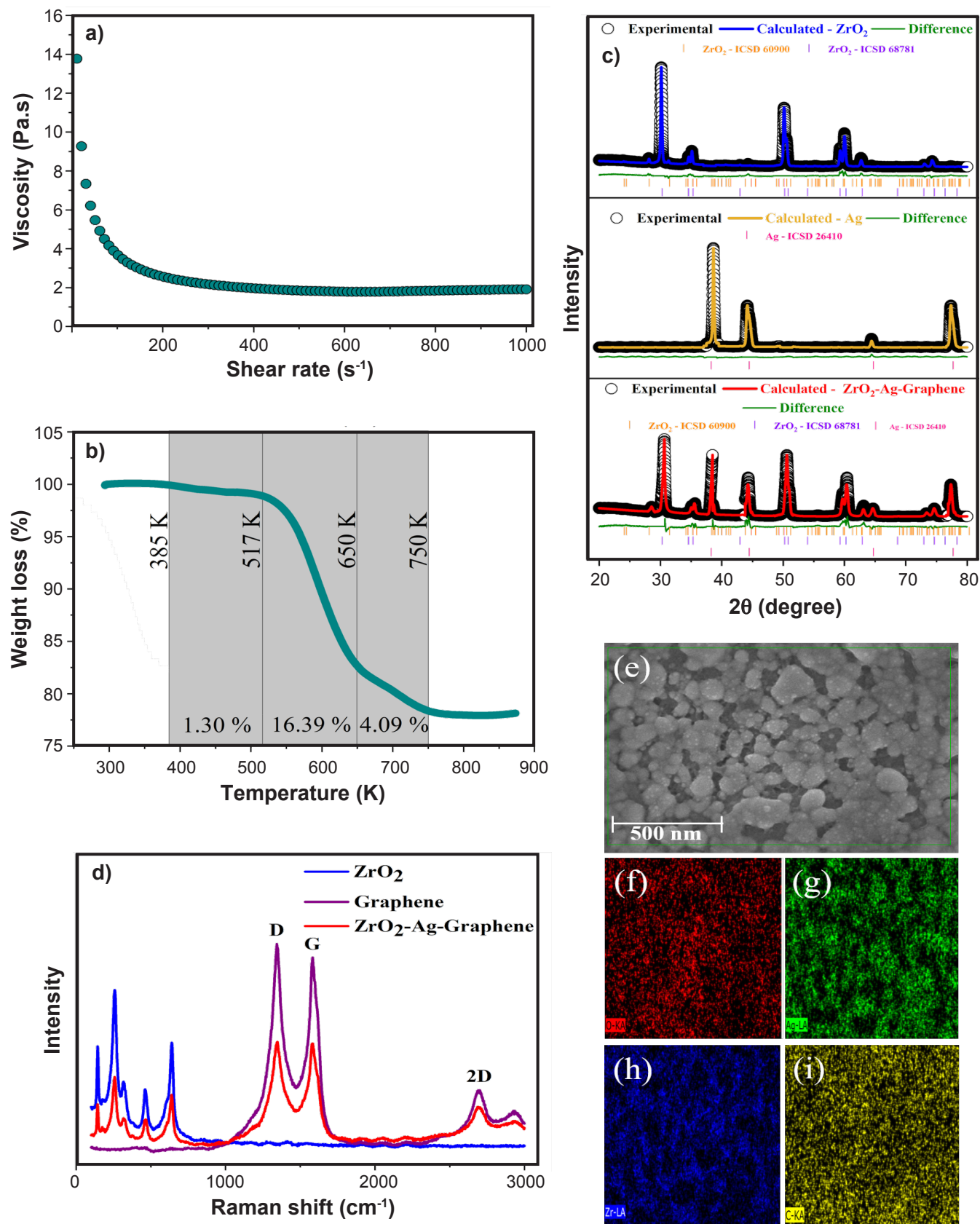


Figure 1: (a) Viscosity of the ceramic suspension as a function of the shear rate. (b) Thermogravimetric analysis curve of the flexible green sheet. (c) Refined XRD patterns of the ZrO_2 sheet, Ag powder, and ZrO_2 -Ag-Graphene sheet. (b) Raman spectrum of the ZrO_2 sheet, graphene powder, and ZrO_2 -Ag-Graphene sheet. FESEM images of (e) ZrO_2 -Ag-Graphene sheet and distribution of elements (f) O, (g) Ag, (h) Zr, and (i) C from EDS mapping.

silver nanoparticles, with d-spacings of approximately 2.36 Å, 2.04 Å, 1.44 Å and 1.23 Å, respectively [33]. Yoon et al., [34] reported that the monoclinic phase is not desired in larger quantities due to significant distortion in the crystal lattice, reducing the density of the stabilized zirconia. Table

2 shows Rietveld refinement's lattice parameters, phase contents, and quality factors (R_{wp} , R_{exp} , and χ^2). Therefore, we note that the values calculated via refinement and the experimental values via XRD show good agreement.

The Raman spectrum of the ZrO_2 sheet, the graphene

Table 2 - Parameters obtained from the Rietveld refinement.

Samples	Phase	wt. (%)	Latt. Par. (Å)	Agreement factors		
				R_{wp} (%)	R_{exp} (%)	χ^2
ZrO_2	M- ZrO_2	22.76	$a = 5.1411(8)$, $b = 5.2090(7)$ $c = 5.1742(7)$	12.93	11.92	1.08
	T- ZrO_2	77.24	$a = b = 3.5902(5)$ $c = 5.1742(7)$			
Ag	C-Ag	100.00	$a = b = c = 4.0817(8)$	12.56	11.84	1.06
	M- ZrO_2	2.41	$a = 5.8225(6)$, $b = 5.0487(8)$ $c = 5.2458(5)$			
ZrO_2 -Ag-Graphene	T- ZrO_2	90.05	$a = b = 3.1275(8)$ $c = 5.8753(6)$	12.74	11.09	1.14
	C-Ag	7.54	$a = b = c = 3.5421(7)$			

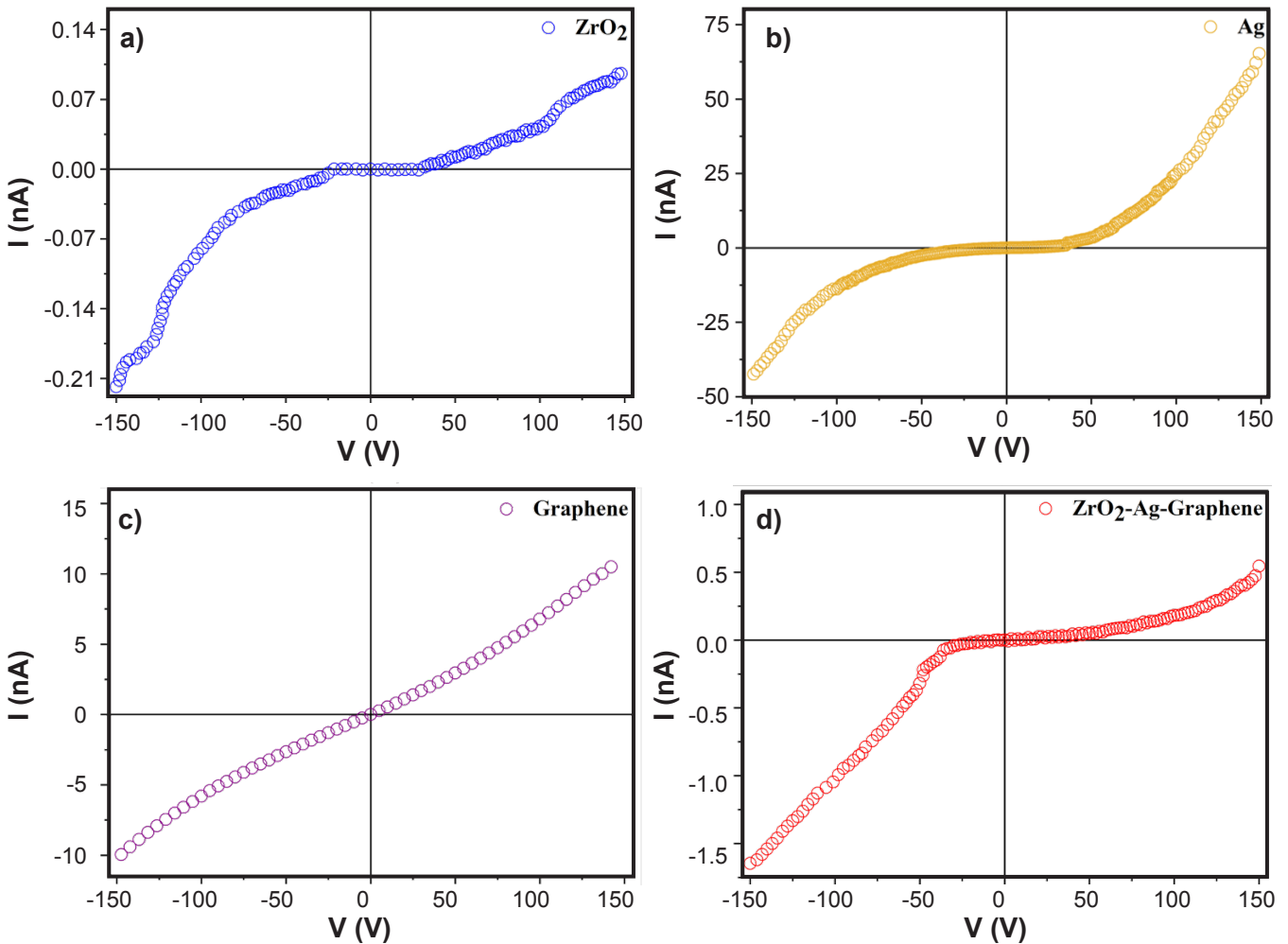


Figure 2: I-V curves of the (a) ZrO_2 sheet, (b) Ag powder, (c) graphene powder, and (d) ZrO_2 -Ag-Graphene sheet.

powder and the ZrO_2 -Ag-Graphene sheet are detailed in Fig. 1d. We observed that the spectrum of the ZrO_2 sheet, whose peaks are in the frequency range of $100\text{--}800\text{ cm}^{-1}$, indicate the presence of the six vibrational modes of tetragonal zirconia: B_{1g} , E_g , B_{1g} , E_g , A_{1g} and E_g [35]. For the graphene powder, we evidenced the presence of three characteristic peaks known as the D (1333 cm^{-1}), G (1587 cm^{-1}), and 2D (2693 cm^{-1}) bands [36]. The appearance of these modes confirms that graphene and ZrO_2 are present in the ceramic sheet. Through FESEM images, we observed the morphology of the ZrO_2 -Ag-Graphene ceramic sheet. Fig. 1e shows grains with varying sizes and irregular geometries, which may be related to the mixing process and heat treatments to which the sheet is subjected [37]. In the EDS images, Fig. 1f-i, we notice a homogeneous distribution of the elements O, Ag, Zr, and C, which confirms the efficiency of the method used.

Finally, we investigated the electrical response, through I-V curves, of the ZrO_2 sheet, the Ag powder, the graphene powder, and the ZrO_2 -Ag-Graphene sheet. The electrical behavior for the ZrO_2 sheet (Fig. 2a) and the Ag powder (Fig. 2b) presents a non-ohmic character, with the electrical resistance measured at low voltage values around $10^9\ \Omega$ and $10^6\ \Omega$, respectively. On the other hand, graphene offers ohmic behavior, and the electrical resistance at low voltage values decreases to around $10^3\ \Omega$, as can be seen in Fig. 2c. The decrease in graphene's electrical resistance is related to the hexagonal rings, in which there are double bonds, allowing electrons to migrate. Furthermore, carbons assume sp^2 hybridization, forming parallel sheets and weaker bonds in different planes, allowing electrons to move between planes; that is, electricity transfer occurs [38].

For the ZrO_2 -Ag-Graphene sheet, Fig. 2d shows a non-ohmic behavior with electrical resistance around $10^9\ \Omega$. Although it is of the same order of magnitude as the ZrO_2 sheet, we observe a decrease in electrical resistance. According to Khan et al. [39], this fact is attributed to the excellent dispersion of Ag and graphene on the surface of the ceramic sheet, as seen in the EDS images.

CONCLUSION

The ZrO_2 -Ag-Graphene sheet presents satisfactory results, such as homogeneity, absence of surface defects, and solid interfacial connection between the grains. Furthermore, we observed a non-ohmic behavior with electrical resistance around $10^9\ \Omega$ with the deposition of silver and graphene on the ZrO_2 structure. Therefore, our results pave the way for using ZrO_2 -Ag-Graphene sheet in high-frequency substrate applications for electronic transmission devices.

ACKNOWLEDGEMENTS

Hugo P. A. Alves acknowledges the Coordination for the Improvement of Higher Education Personnel (CAPES, 88887.800034/2022-00) for the financial support. Paulo H. Chiberio acknowledges Brazil's National Research Council (CNPq, 164013/2021-0) for the financial support.

REFERENCES

- [1] Tripathi, H., Kumar, S., Bhardwaj, S., Sharma, J.D.. Impact of Nd^{3+} , Er^{3+} ions on the structural, morphological and opto-electrical properties of $\text{ZrO}_2/\text{La}_2\text{O}_3$ doped Y_2O_3 ceramics. *Ceramics International* 2024;**50**(2):18549–18558.
- [2] Madhusudhana, H., Shobhadevi, S., Nagabhushana, B., Krishna, R.H., Murugendrappa, M., Nagabhushana, H. Structural characterization and dielectric studies of Gd doped ZrO_2 nano crystals synthesized by solution combustion method. *Materials Today: Proceedings* 2018;**5**(10):21195–21204.
- [3] Patil, S.R., Barhate, V.N., Patil, V.S., Agrawal, K.S., Mahajan, A.M.. The effect of post-deposition annealing on the chemical, structural and electrical properties of Al/ $\text{ZrO}_2/\text{La}_2\text{O}_3/\text{ZrO}_2/\text{Al}$ high-k nanolaminated mim capacitors. *Journal of Materials Science: Materials in Electronics* 2022;**33**(14):11227–11235.
- [4] Wang, X., Chen, J., Zheng, M., Yang, F., Shao, D., Hao, Y., et al. Improvement of the energy storage performance in $\text{Pb}_{0.88}\text{La}_{0.12}\text{ZrO}_3$ thin films by inserting ZrO_2 layer. *Physica B: Condensed Matter* 2023;**665**:415073.
- [5] Attar, A., Alharthy, R.D., Zwawi, M., Algarni, M., Albatati, F., Bassyouni, M., et al. Fabrication, characterization, TD-DFT, optical and electrical properties of poly (aniline-co-para nitroaniline)/ ZrO_2 composite for solar cell applications. *Journal of Industrial and Engineering Chemistry* 2022;**109**:230–244.
- [6] Cai, H., Tuokedaerhan, K., Lu, Z., Zhang, R., Du, H. Effect of annealing temperature on the structural, optical, and electrical properties of Al-doped ZrO_2 gate dielectric films treated by the Sol–Gel method. *Coatings* 2022;**12**(12):1837.
- [7] Mohammed, M.A., Salman, S.R., Wasna'a, M.A. Structural, optical, electrical and gas sensor properties of ZrO_2 thin films prepared by sol-gel technique. *NeuroQuantology* 2020;**18**(3):22.
- [8] Sadoun, A., Najjar, I., Abd-Elwahed, M., Meselhy, A.. Experimental study on properties of Al– Al_2O_3 nanocomposite hybridized by graphene nanosheets. *Journal of Materials Research and Technology* 2020;**9**(6):14708–14717.
- [9] Xu, F., Yuan, Y., Wu, D., Zhao, M., Gao, Z., Jiang, K.. Synthesis of $\text{ZnO}/\text{Ag}/\text{Graphene}$ composite and its enhanced photocatalytic efficiency. *Materials Research Bulletin* 2013;**48**(6):2066–2070.
- [10] Faraji, M., Mohaghegh, N.. Ag/ TiO_2 -nanotube plates coated with reduced graphene oxide as photocatalysts. *Surface and Coatings Technology* 2016;**288**:144–150.
- [11] Routray, K.L., Saha, S., Behera, D. Insight into the anomalous electrical behavior, dielectric and magnetic study of ag-doped cofe_2o_4 synthesised by okra extract-assisted green synthesis. *Journal of Electronic Materials* 2020;**49**:7244–7258.
- [12] Routray, K.L., Saha, S.. Graphene nanoplatelets anchored into ag doped spinel cofe_2o_4 nanohybrid: Synthesis, structural, electrical, superior dielectric and room temperature induced ferromagnetism performance for

high frequency device application. *Diamond and Related Materials* 2024;**141**:110680.

[13] Ahmad, M., Ahmed, E., Hong, Z., Khalid, N., Ahmed, W., Elhissi, A. Graphene–Ag/ZnO nanocomposites as high performance photocatalysts under visible light irradiation. *Journal of Alloys and Compounds* 2013;**577**:717–727.

[14] Sadoun, A., Najjar, I., Wagih, A.. Electroless-plating of Ag nanoparticles on Al_2O_3 and graphene Nano sheets (GNs) for improved wettability and properties of Al– Al_2O_3 /GNs nanocomposites. *Ceramics International* 2021;**47**(8):10855–10865.

[15] Correa, M., Araujo, M., Acchar, W., Souza, A., Melo, A., Bohn, F. ZrO_2 tape as flexible substrate to artificially nanostructured materials. *Materials Letters* 2017;**196**:69–73.

[16] Duntu, S.H., Ahmad, I., Islam, M., Boakye-Yiadom, S.. Effect of graphene and zirconia on microstructure and tribological behaviour of alumina matrix nanocomposites. *Wear* 2019;**438**:203067.

[17] Junior, S.F., Acchar, W., Dantas, S., Chiberio, P., Alves, H., Bomio, M., et al. Enhanced high-frequency dielectric properties in ZrO_2 – BaTiO_3 ceramic heterostructures. *Ceramics International* 2023;**49**(22):36025–36030.

[18] Liu, Y., Tian, J., Wei, L., Wang, Q., Wang, C., Yang, C.. A novel microwave-assisted impregnation method with water as the dispersion medium to synthesize modified $\text{g-C}_3\text{N}_4/\text{TiO}_2$ heterojunction photocatalysts. *Optical Materials* 2020;**107**:110128.

[19] Sezgin, A., Ctvrtl'ík, R., Vaclavek, L., Toma'st'ík, J., Nozka, L., Mensur, E., et al. Optical, structural and mechanical properties of TiO_2 and TiO_2 – ZrO_2 thin films deposited on glass using magnetron sputtering. *Materials Today Communications* 2023;**35**:106334.

[20] Alves, H., Costa, A., Carvalho, B., Bohn, F., Correa, M., Acchar, W. Incorporating graphene into a sintered ceramic tape: structural and magnetic properties of a zirconia-graphene composite. *Materials Letters* 2020;**270**:127689.

[21] Chiberio, P. H., Alves, H. P., Junior, R.A., Neto, J. M. D., Acchar, W.. Al_2O_3 dielectric ceramic tapes containing HBN for applications on high-frequency substrates. *Ceramics International* 2024;**50**(2):2864–2870.

[22] Li, W., Guo, C., Cui, C., Bao, J., Zhang, G., Zhang, Y., et al. Microstructure evolution and performance improvement of silicon carbide ceramics via impregnation method. *Materials* 2022;**15**(5):1717.

[23] Correa, M.A., Ferreira, A., Tromer, R.M., Machado, L.D., Gamino, M., Franca Junior, S.A., et al. Improving the room-temperature ferromagnetism in ZnO and low-doped ZnO: Ag films using GLAD sputtering. *Materials* 2021;**14**(18):5337.

[24] Costa, A., Alves, H., Correa, M., Bohn, F., Acchar, W. Iron oxide/PVA flexible magnetic tape engineered by microwave combustion and tape casting. *Materials Chemistry and Physics* 2019;**232**:1–5.

[25] Zhao, H., Tang, F., Xie, Y., Wen, Z., Tian, K., Nie, X., et al. Fabrication and rheological behavior of tape-casting slurry for ultra-thin multilayer transparent ceramics. *International Journal of Applied Ceramic Technology*

2020;**17**(3):1255–1263.

[26] Goulart, C., de Souza, D.. Critical analysis of aqueous tape casting, sintering, and characterization of planar Yttria-Stabilized Zirconia electrolytes for SOFC. *International Journal of Applied Ceramic Technology* 2017;**14**(3):413–423.

[27] Rahmawati, F., Zuhri, N., Nugrahaningtyas, K.D., Arifah, S.K.. Yttria-stabilized zirconia (YSZ) film produced from an aqueous nano-YSZ slurry: preparation and characterization. *Journal of Materials Research and Technology* 2019;**8**(5):4425–4434.

[28] Chan, M.S., Baldovi, H.G., Dennis, J.. Enhancing the capacity of oxygen carriers for selective oxidations through phase cooperation: bismuth oxide and ceria–zirconia. *Catalysis Science & Technology* 2018;**8**(3):887–897.

[29] Alves, H.P., Alves Junior, R., Carvalho, B.R., Correa, M.A., Acchar, W. Structural and magnetic behavior of zirconia-magnetic particles and zirconia-graphene composite ceramics. *Journal of the American Ceramic Society* 2021;**104**(11):5711–5718.

[30] Dudek, K., Podworny, J., Dulski, M., Nowak, A., Peszke, J. X-ray investigations into silica / silver nanocomposite. *Powder Diffraction* 2017;**32**(S1):S82–S86.

[31] Kuo, C.W., Lee, K.C., Yen, F.L., Shen, Y.H., Lee, H.E., Wen, S.B., et al. Growth kinetics of tetragonal and monoclinic ZrO_2 crystallites in 3 mol% yttria partially stabilized ZrO_2 (3Y-PSZ) precursor powder. *Journal of Alloys and Compounds* 2014;**592**:288–295.

[32] Dwivedi, R., Maurya, A., Verma, A., Prasad, R., Bartwal, K.. Microwave assisted sol–gel synthesis of tetragonal zirconia nanoparticles. *Journal of Alloys and Compounds* 2011;**509**(24):6848–6851.

[33] Majeed Khan, M.A., Kumar, S., Ahamed, M., Alrokayan, S.A., AlSalhi, M.S.. Structural and thermal studies of silver nanoparticles and electrical transport study of their thin films. *Nanoscale Research Letters* 2011;**6**:1–8.

[34] Yoon, S., Noh, T., Kim, W., Choi, J., Lee, H. Structural parameters and oxygen ion conductivity of Y_2O_3 – ZrO_2 and MgO – ZrO_2 at high temperature. *Ceramics International* 2013;**39**(8):9247–9251.

[35] Djurado, E., Boulc'h, F., Dessemond, L., Rosman, N., Mermoux, M.. Study on aging of tetragonal zirconia by coupling impedance and Raman spectroscopies in water vapor atmosphere. *Journal of the Electrochemical Society* 2004;**151**(5):A774–A780.

[36] Zuluaga-Gomez, C.C., Plaza-Rivera, C.O., Tripathi, B., Katiyar, R.K., Pradhan, D.K., Morell, G., et al. Holey Graphene/Ferroelectric/Sulfur composite cathodes for high-capacity lithium–sulfur batteries. *ACS omega* 2023;**8**(14):13097–13108.

[37] Lin, F., Zhu, Z., Zhou, X., Qiu, W., Niu, C., Hu, J., et al. Orientation control of graphene flakes by magnetic field: broad device applications of macroscopically aligned graphene. *Advanced Materials* 2017;**29**(1):1604453.

[38] Ke, Q., Wang, J.. Graphene-based materials for supercapacitor electrodes—A review. *Journal of Materiomics* 2016;**2**(1):37–54.

[39] Khan, M.E., Khan, M.M., Cho, M.H.. Biogenic synthesis of a Ag–graphene nanocomposite with efficient photocatalytic degradation, electrical conductivity and

photoelectrochemical performance. New Journal of Chemistry 2015;**39**(10):8121–8129.

(Rec. 08-Aug-2024, Rev. 25-Oct-2024, Ac. 26-Nov-2024)

(AE: Rafael Salomão)

